RSC Advances

REVIEW

View Article Online
View Journal | View Issue

Cite this: *RSC Adv.*, 2024, **14**, 38480

Application of rare earth elements in dual-modality molecular probes

Jie-Fang He, †[a] Wen-Wen Yang,†[ad] Wen-Xuan Quan,[b] Yue-Chun Yang,[c] Zhengwei Zhang[d] and Qing-Ying Luo *[d]

Received 10th July 2024
Accepted 18th November 2024

DOI: 10.1039/d4ra04987j

rsc.li/rsc-advances

The unique 4f subshell electronic structure of rare earth elements endows them with exceptional properties in electrical, magnetic, and optical domains. These properties include prolonged fluorescence lifetimes, large Stokes shifts, distinctive spectral bands, and strong resistance to photobleaching, making them ideal for the synthesis of molecular probes. Each imaging technique possesses unique advantages and specific applicabilities but also inherent limitations due to its operational principles. Dual-modality molecular probes effectively address these limitations, particularly in applications involving high-resolution Magnetic Resonance Imaging (MRI) such as MRI/OI, MRI/PET, MRI/CT, and MRI/US. This review summarizes the applications, advantages, challenges, and current research status of rare earth elements in these four dual imaging modalities, providing a theoretical basis for the future development and application of rare earth elements in the field of dual-modality molecular probes.

1. Introduction

Yttrium (Y), one of the rare earth elements, was first discovered in 1794 by Finnish chemist Johan Gadolin, and was originally named "yttria". The term "rare earth elements" was later used to describe a group of elements with similar properties.[1] According to the International Union of Pure and Applied Chemistry (IUPAC), rare earth elements include 15 lanthanides and yttrium (Y), with scandium (Sc) often discussed alongside them, although its role in dual-modality molecular probes is relatively limited.[2–4] The unique characteristics of rare earth elements, particularly their partially filled 4f electron orbitals, give them distinct electrical, magnetic, and optical properties, making them ideal for applications in dual-modality molecular probes.

China, as the world's largest holder of proven rare earth resources, plays a leading role in the global supply chain.[5] This dominance has had a profound impact on international markets and technological development, especially in the field of dual-modality molecular probes. This review summarizes the applications of rare earth elements in dual-modality molecular probes, highlighting their advantages in imaging and diagnostics, as well as the challenges faced in their utilization. The aim is to provide a theoretical foundation and direction for future research in this area.

2. Characteristics of REE

The electron configuration of rare earth elements can be summarized as $[Xe]4f^{0-14}5d^{0-1}6s^2$, indicating that the 4f orbital can accommodate 0 to 14 electrons, the 5d orbital 0 to 1 electron, and the 6s orbital typically holds 2 electrons.[6] The electron configuration of lanthanide elements is commonly abbreviated as $[Xe]4f^n5d^{0-1}6s^2$, where n ranges from 1 to 14. This abbreviation helps to clearly indicate the filling of the 4f electrons in these elements. The phenomenon known as lanthanide contraction is mainly due to the $5s^2$ and $5p^6$ electrons providing some shielding, but this shielding is insufficient to fully counterbalance the increase in core attraction as more electrons fill the 4f orbitals.[7] This results in an increased effective nuclear charge and a gradual decrease in atomic radius.[8] Lanthanide contraction is characterized by a steady decrease in the size of the lanthanide cations (or atoms) as the atomic number increases, contrary to what might be expected.[9] This effect is crucial for understanding the properties of these elements, especially in applications related to medical imaging, where precise electronic structure and physical properties are critical.[10]

Rare earth elements possess unfilled 4f orbitals, and their 4f electrons are shielded by outer $5s^2$ and $5p^6$ electrons. This configuration offers unique advantages in optics and magnetic resonance applications: (1) strong paramagnetism; (2) long fluorescence lifetimes, typically ranging from 100 to 1000 microseconds; (3) significant Stokes shifts, usually exceeding 200 nm, which helps mitigate non-specific fluorescence interference; (4) a broad excitation spectrum, facilitating excitation at multiple wavelengths; (5) a narrow emission spectrum, where

[a]*School of Life Sciences, Guizhou Normal University, Guiyang 550025, China*
[b]*Provincial Key Laboratory of Mountainous Ecological Environment, Guizhou Normal University, Guiyang, 550025, China*
[c]*Guizhou University of Traditional Chinese Medicine, Guiyang, 550025, China*
[d]*School of Food and Drug, Shenzhen Polytechnic University, Shenzhen 518055, China. E-mail: Luoqingying@szpu.edu.cn*
† Jie-Fang He and Wen-Wen Yang contributed equally.

Table 1 The difference between atoms and ions of rare earth elements

REE	Atoms	Ions
Physical state	Ln (solid)	Ln^{3+}, Ln^{4+} (in solution)
Electron shells	Complete	Incomplete
Chemical reactivity	High, easily to be oxidated	Low, stable ions form
Toxicity	Yes	Reduced toxicity through complexation
Fluorescence	No	Yes (*e.g.*, Eu^{3+}, Tb^{3+})
Magnetic	—	Paramagnetic (*e.g.*, Gd^{3+})
Application	Limited	Medical imaging, drug delivery and therapy

distinct peaks from different transitions are easily distinguishable, enhancing resolution and reducing background noise (Table 1).[7,11–15]

Rare earth complexes serve as a vast reservoir of luminescent materials, playing a pivotal role among developed luminous substances. The luminescence type and performance of these complexes are intricately linked to the 4f electron configuration of rare earth ions and their diverse transition processes. The majority of rare earth ions exhibit luminescence from forbidden 4f–4f transitions, characterized by low absorption coefficients and weak ultraviolet light absorption.[16–18] These transitions produce narrow spectral bands and stable emission wavelengths, maintaining the monochromatic nature of the luminescence, which is advantageous for high-precision imaging technologies. However, rare earth ions have weak direct light absorption capabilities, making them challenging to excite directly, which results in low luminescence efficiency. By using chromophores as ligands to form stable complexes, the ligands absorb energy and then transfer it to the rare earth ions, allowing them to transition from the ground state to an excited state and emit photons (Fig. 1).[19] In this process, chromophores, referred to as "antenna groups," enhance the sensitization of rare earth ions, a phenomenon known as the "antenna effect".[20] In 1942, Weissman[21] first demonstrated that exciting lanthanide ion complexes to an excited state induces luminescence at the metal centre. Additionally, the sensitization process offers two benefits: firstly, the Stokes shift of lanthanide ions upon direct excitation is negligible, but the unique properties of the 4f orbitals cause the ligand-induced Stokes shift to be significantly larger than that of organic fluorophores,

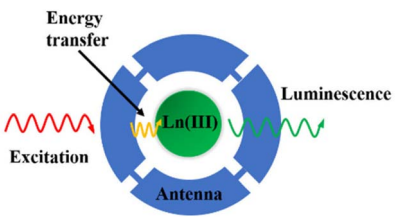

Fig. 1 The antenna effect (adapted with permission ref. 19 with permission from the American Chemical Society, Copyright 2009).

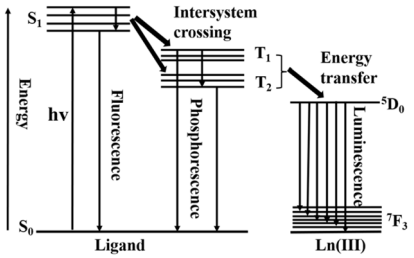

Fig. 2 Schematic energy level diagram for a rare earth chelate possessing low-lying 4f electronic states (adapted with permission ref. 25 with permission from the American Chemical Society, Copyright 2012).

making it easier to distinguish the emitted light spectrum; secondly, lanthanide ions are excellent quenchers of triplet states, thus significantly reducing photobleaching.

The widely accepted mechanism for energy transfer from organic ligands to lanthanide ions was proposed by Crosby and Whan in1961.[22–24] Under UV radiation, the organic ligands of lanthanide complexes are excited from the ground singlet state (S_0) to the first excited singlet state (S_1), leading to potential energy emissions. In one scenario, the energy can radiate as the ligand transitions back to the ground state, emitting characteristic fluorescence of the organic ligand. Alternatively, energy may be transferred through a non-radiative process to the triplet excited state (T_1), where it can either radiate and release energy as characteristic phosphorescence of the ligand or continue through a non-radiative energy transfer to excite the lanthanide ion. The lanthanide ion then emits long-lived luminescence as it returns from the excited state to the ground state, producing photons (Fig. 2).[25] Research has shown that energy transfer from organic ligands to lanthanide ions is 10^3 to 10^5 times more efficient than direct excitation of the lanthanide ions.[26] The ability of lanthanide ions to form complexes with organic molecules significantly reduces toxicity and enhances biocompatibility, which is crucial for targeted drug delivery and cancer therapy. However, the characteristics of lanthanide ions in their ionic state are difficult to achieve in their atomic state due to the lack of a stable electronic environment.[15]

3. Dual-modality molecular probes

Molecular imaging, an integral part of biomedical imaging, facilitates the visualization, characterization, and quantitative measurement of biological processes *in vivo* using non-invasive, real-time, and three-dimensional techniques.[27–31] This field extends broadly to technologies that monitor and document the spatial and temporal behaviours of molecular and cellular activities, applicable across biochemistry, biology, and clinical diagnostics and treatments.[32,33] Particularly, the application of REE enhances dual-modality molecular probes, integrating multiple imaging techniques to provide more comprehensive diagnostic data. Prominent imaging techniques enhanced by rare earth elements include: (1) Magnetic Resonance Imaging (MRI); (2) Optical Imaging (OI), further divided into

Table 2 Comparison of different imaging techniques

Imaging technique	Space resolution	Penetration depth	Time	Sensitivity (mol L^{-1})
MRI	20–100 μm	No limit	min–h	10^{-3}–10^{-5}
OI	>0.3 μm	120 mm	s–min min–h	10^{-10}–10^{-12}
PET	1–2 mm	No limit	s–min	10^{-11}–10^{-12}
SPECT	0.5–1 mm	No limit	min	10^{-9}–10^{-11}
CT	50–200 μm	No limit	min	10^{-2}–10^{-4}
US	50–500 μm	mm–cm	s–min	10^{-3}–10^{-4}

subcategories such as bioluminescence, fluorescence imaging (FI), photoacoustic imaging (PAI), and optical coherence tomography; (3) Radioisotope Imaging, which comprises Single-photon Emission Computed Tomography (SPECT) and Positron Emission Tomography (PET); (4) Computed Tomography (CT); and (5) Ultrasonic Imaging (US).[34–36] These modalities, particularly when combined with the unique properties of REE, offer significant improvements in the sensitivity and specificity of molecular probes (Table 2).

Among current imaging technologies, MRI is particularly noteworthy for its widespread use, facilitated by its capability to deliver high-quality, high-resolution three-dimensional images of soft tissues. This is achieved with unlimited penetration depth and exceptional soft tissue contrast, advantages that make MRI indispensable in the realm of medical imaging.[37–39] Utilizing the principles of Nuclear Magnetic Resonance (NMR), MRI operates without generating ionizing radiation, ensuring a safer imaging process.[40,41] The technique relies on the relaxation rates of water molecule protons, with variations in water density, proton relaxation times, or diffusion rates used to differentiate between tissue types. The contrast in MRI images can be significantly enhanced through the application of paramagnetic molecular probes, often composed of REE, which are efficient at increasing the relaxation rate.[42]

However, the inherent low sensitivity of MRI limits its application scope, prompting the integration of MRI with other imaging technologies to enhance diagnostic capabilities. This integration aims to reduce false positives and negatives, thus improving diagnostic accuracy and reliability, crucial in overcoming the limitations of single-modality imaging.[43] For instance, the combination of MRI and Optical Imaging (OI) compensates for the low sensitivity of MRI and the spatial resolution limitations of OI. Both modalities benefit immensely from the complementary strengths of REE in these dual-modality molecular probes. The application of REE in MRI/OI dual-modality imaging is a significant area of current research; similarly, the combination of MRI with PET addresses both MRI's sensitivity issues and PET's low spatial resolution while enabling quantitative analysis. CT, while being one of the most common and cost-effective imaging techniques providing high-resolution 3D tomographic data, offers limited soft tissue resolution unlike.[44] MRI, which is enhanced by the superior contrast provided by REE.[45,46] Ultrasound (US) imaging, recognized for being safe, non-invasive, portable, economical, and easy to use, suffers from low sensitivity and limited penetration depth; integrating MRI with US in dual-modality imaging can partly resolve these issues of spatial resolution.[47,48]

Molecular probes constitute a pivotal component of contemporary molecular imaging techniques, acting as specialized agents that selectively accumulate in targeted biological areas to produce detectable signals for advanced imaging systems. Optimal molecular probes are characterized by several critical biological properties: (1) robust stability and high biocompatibility, enabling seamless integration into physiological processes; (2) minimal molecular weight, facilitating their diffusion through complex physiological barriers; (3) the capability for prolonged metabolic persistence *in vivo*, allowing extended visualization of specific targets; and (4) the feasibility of synthesis.[49–52] This discourse will focus specifically on the utilization of REE in enhancing the functionality of dual-modality molecular probes. Rare earth complexes, with their distinctive electronic configurations and photophysical properties, significantly augment the diagnostic capabilities of such probes. We will delve into the detailed applications and ongoing advancements of these elements in refining both the accuracy and the utility of diagnostic and therapeutic modalities.

4. Application of rare earth complexes as dual-modality molecular probes

In addition to their unique optical properties, rare earth complexes can be modified to enhance their hydrophilicity and biocompatibility. This makes them particularly advantageous for *in vivo* imaging and detection, and they are extensively used in bioimaging and biosensing. This section briefly summarizes the applications of rare earth complexes in various dual-modality imaging techniques (Table 3).

4.1. Application of rare earth complexes as dual-modality molecular probes in MRI/OI

Optical Imaging (OI) is a non-invasive technique known for its high sensitivity and specificity, as well as its capacity for real-time imaging. However, its effectiveness is limited by poor tissue light penetration.[33,85] By combining Magnetic Resonance Imaging (MRI) with Optical Imaging, dual-modality imaging offers synergistic advantages that neither modality can achieve

Table 3 Rare earth probes for dual-mode imaging

Mode of imaging	Probe	Rare earth element	Ref.
MRI/OI	EDTA-Gd(III)-CL	Gd	53
	Gd(III)-DO3A	Gd	54
	YbL_{Gal}^5	Yb	55
	Per-6-Diimi [Gd $(NO_3)_4$]	Gd	56
	Gd-CQDs@N-Fe_3O_4	Gd	57
	Au@Gd_2O_3@*m*SiO_2@ PEG-FA	Gd	58
	Gd-FPNPs	Gd	59
	YbL^3, NdL^3, GdL^3	Yb, Nd, Gd	60
	FA-PEI-$NaGdF_4$: Eu	Eu	61
	Eu(III)-DTPA-BC_{10}coumarin	Eu	62
	Ln(III)-DTPA-BC_{10}coumarin	Ln	62
MRI/PET	Gd_6L [PEG_{12}c(RGDyK)]$_3$^{68}Ga	Gd	63
	Gd@C_{82}-Ala-PEG-cRGD-NOTA-^{64}Cu	Gd	64
	HyCoS NPs	Gd	65
	Fmoc-D-Lys (La-DOTA)-Lys (Gd-DOTA)-NH_2	La, Gd	66
	Gd (DO3A-SA)-Ga (AAZTA)	Gd	67
	^{68}Ga-AGuIX-DOTA-Gd	Gd	68
MRI/CT	Gd-PAA-Au	Gd	69
	GBCAs-BP	Gd	70
	CDs: Gd, Dy-TAT@Exo-RGD	Dy, Gd	71
	$NaGdF_4$: Dy@PPF	Dy, Gd	72
	ZnO: Gd, Yb NPs	Yb, Gd	73
	$NaGdF_4$: Dy NPs	Dy, Gd	74
	Gd: AuNPs@SF	Gd	75
	FA-Gd-Au PENPs	Gd	76
	RGD-Gd-Au DEN-PS	Gd	77
	pEGFR-targeted Ba_2GdF_7 NPs	Gd	78
	Gd/CeO_2-ZrO_2/DOX-PEG	Ce, Gd	79
	IC-GNPs	Gd	80
MRI/US	PFOB@PLA/GO/Gd-DTPA NCs	Gd	81
	PFP/GdDTPA/ICG@PLGA NPs	Gd	82
	Gd/PFH@Alg-FA	Gd	83
	Gd-DOTA/DOX@PFH NDs	Gd	84

alone, effectively overcoming their individual limitations and maximizing their strengths.[86] Among dual-modality imaging approaches, MRI/OI is the most rapidly advancing and extensively studied, finding applications in both biomedical research and clinical practice.[87] MRI/OI dual-modality molecular probes can be categorized into small molecule probes and nanoparticle probes, each playing a crucial role in enhancing diagnostic capabilities.[88] Small molecule probes offer significant benefits due to their rapid metabolism in the body, their ability to quickly disseminate across various organs and tissues, and their low biotoxicity.[89] Meanwhile, nanoparticle probes, which frequently incorporate REE, elevate diagnostic accuracy with their considerable payload capacity and adjustable surface properties, facilitating precise targeted delivery and enhanced biocompatibility. These attributes make them exceptionally effective in dual-modality molecular probes, markedly improving the resolution and efficacy of medical diagnostics and treatments.[90–92] In 1988, the first molecular probe containing gadolinium Gd(III) was approved for clinical use. Today, gadolinium complexes (such as DOTA-Gd^{3+} and DTPA-Gd^{3+}) are the most commonly used probes in MRI due to their high stability and low biotoxicity.[93]

One of the current research hotspots in MRI/OI probes is the development of compounds based on Gd(III). Wang[53] reported a novel MRI/fluorescence dual-modality molecular probe composed of an EDTA-Gd(III) complex and a coumarin-based fluorescent group (CL). In this probe, coumarin serves as the chromophore due to its long-wavelength absorption and emission, high fluorescence quantum yield, and good biocompatibility. Ethylenediaminetetraacetic acid (EDTA) acts as a chelating agent, mitigating the toxicity of free gadolinium (Gd(III)) by providing four oxygen donors and two nitrogen donors, thus forming a highly stable complex, EDTA-Gd(III). Experimental results demonstrate that EDTA-Gd(III)-CL is a fluoride ion-responsive probe. In the presence of fluoride ions, the EDTA-Gd(III)-CL aqueous solution triggers the release of CL, which binds to Gd(III), thereby activating longitudinal relaxation (r_1) and fluorescent responses. Using organic fluorescent dyes as chromophores to prepare molecular probes is a simple, versatile, and non-destructive method that offers real-time, *in situ*, and dynamic information.[94] However, these dyes have inherent limitations: they typically have low absorption coefficients and weak signals, which can reduce sensitivity in applications. Furthermore, organic fluorescent dyes suffer from poor photobleaching resistance, limiting their use in long-term tracking, and their short fluorescence lifetimes also pose a significant drawback in practical applications.[95] To address these issues, it is worth considering the use of quantum dots

(QDs) as chromophores, as they exhibit strong resistance to photobleaching and high quantum yields.[95]

Compared to ion-responsive molecular probes, enzyme-responsive molecular probes offer higher imaging efficiency due to their ability to specifically recognize substrates. Enzymes play crucial roles in many vital biological activities and physiological processes within organisms, and changes in their levels are often closely associated with disease progression. For instance, the overexpression of specific enzymes accompanies the development of various cancers, making these enzymes viable biomarkers for certain cancers. Probes can not only visually reflect the levels of these enzymes within the body but also facilitate optical imaging to guide the surgical removal of diseased tissues. Jouclas[55] reported on a β-galactosidase-responsive probe, YbL_{Gal}^5, which employs 1,4,7,10-tetraazacyclododecane-1,4,7-triacetic acid (DO3A) as the chelating agent for ytterbium (Yb), a pyridine derivative as the chromophore, and β-galactose as the trigger. Cleaved by β-galactosidase, the YbL_{Gal}^5 probe responds specifically, visualizing overexpressed β-galactosidase in samples through various imaging modalities, thereby enhancing the imaging signal of cancer cells. This probe exemplifies the application potential of lanthanide complexes in dual-modality molecular probes, particularly in the precise detection and treatment of cancer.

Advancements in technology have broadened the scope of molecular probes to include both diagnostic and therapeutic uses. Yin[58] crafted a highly stable and safe integrated nanoprobe, Au@Gd_2O_3@mSiO_2@PEG-FA (Fig. 3), composed of gold nanorods coated in mesoporous silica. These rods are loaded with ultrafine Gd_2O_3 nanoparticles *via* laser ablation in liquid (LAL), and subsequently, the silica surface is conjugated with FA-PEG. Density functional theory (DFT) calculations confirm the nanoprobe's high structural stability. Both *in vitro* and *in vivo* experiments have shown that after photothermal therapy (PTT) treatment, this probe effectively cured mice with transplant tumours of 10 to 12 mm in size. Furthermore, the ultrafine Gd_2O_3 nanoparticles can detach from the probe and be swiftly excreted through the kidneys, significantly reducing the long-term toxicity risks associated with gadolinium-based nanoparticles, and thus achieving excellent multimodal imaging and photothermal treatment outcomes.

In the realm of MRI/OI dual-modality molecular probes, both small molecule and nanoparticle varieties that incorporate REE demonstrate enhanced longitudinal relaxivity compared to single-modality probes. Despite these advancements, these dual-modality probes face challenges such as suboptimal biocompatibility, stability, and aqueous solubility. Future efforts are directed toward developing dual-modality probes with superior relaxivity and improved fluorescence stability, leveraging REE to meet the evolving needs of various application domains.

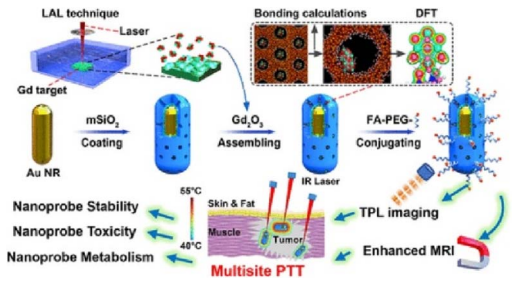

Fig. 3 Synthesis and mechanism of MRI/OI bimodal molecular probe Au@Gd_2O_3@mSiO_2@PEG-FA (adapted with permission ref. 58 with permission from the American Chemical Society, Copyright 2019).

4.2. Application of rare earth complexes as dual-modality molecular probes in MRI/PET

PET employs radiotracers that decay through positron emission, providing critical insights into biological processes with high molecular sensitivity.[96] However, despite its capabilities, PET often suffers from limited spatial resolution, and its imaging output generally lacks the necessary clinical details.[97] Utilizing PET/CT can enhance the localization of abnormalities detected by PET, but this integration raises concerns about radiation exposure, particularly in children who are more vulnerable to radiation effects.[98] Chawla[99] reported that in pediatric PET/CT, the CT component contributed significantly more to radiation exposure (20.3 mSv) than the PET component (4.6 mSv). In contrast, MRI, which does not involve ionizing radiation and offers superior spatial resolution and soft tissue contrast, can be paired effectively with PET. When REE are utilized in the development of MRI/PET dual-modality molecular probes, they significantly enhance the overall imaging performance, combining the best of both modalities for a more comprehensive diagnostic approach.

To address these challenges, MRI is combined with PET, taking advantage of MRI's lack of ionizing radiation and superior spatial resolution and soft tissue contrast.[100] The integration of MRI with PET has led to the development of dual-modality molecular probes that incorporate REE, significantly enhancing overall imaging performance. Since their introduction in 1997, MRI/PET dual-modality molecular probes have undergone extensive research and practical application.[101] Kumar[63] successfully synthesized the PET/MRI dual-modality probe Gd_6LGa, which has a dendritic structure with 1,4,7-triazacyclononane-*N*,*N*′,*N*″-triacetic acid (NOTA) as the core. It is peripherally modified with six 1,4,7,10-tetraazacyclododecane-1,4,7,10-tetraacetic acid (DOTA) moieties, each chelating rare earth elements gadolinium (Gd) and gallium (Ga) respectively. Animal studies assessing the *in vivo* tissue distribution, pharmacokinetics, and stability of Gd_6LGa have demonstrated its excellent stability and pharmacokinetic properties. Furthermore, targeted modifications of Gd_6LGa enable dual-modality imaging of tumours in U87-MG glioblastoma-bearing mice. Chen[64] further innovated by developing a dual-modality molecular probe using a nanocarrier, Gd@C_{82}-Ala-PEG-cRGD-NOTA-^{64}Cu. Gd@C_{82}-Ala exhibits significant anticancer activity. The probe is chemically modified with an eight-arm polyethylene glycol amine (8-arm-PEG-NH_2) to enhance biocompatibility and provide active sites for tumour ligand (cRGD) and PET isotope (^{64}Cu) attachment. Its targeting capability towards U87-MG cells was evaluated using flow cytometry, confocal fluorescence microscopy, and dynamic cell interaction assays.

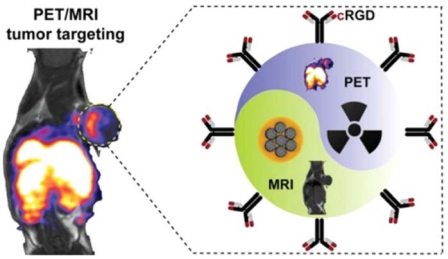

Fig. 4 Targeted imaging of U87-MG-bearing mice is performed with a PET/MRI probe Gd@C_{82}-Ala-PEG-cRGD-NOTA-^{64}Cu (adapted with permission ref. 64 with permission from American Chemical Society, Copyright 2019).

Additionally, the probe was labelled with ^{89}Zr for metabolic studies lasting up to 30 days. Cellular and animal experiments indicate that this probe holds broad prospects for clinical translation, especially in tumour imaging and treatment monitoring in U87-MG glioblastoma-bearing mice (Fig. 4).

Currently, MRI/PET dual-modality molecular probes, often incorporating rare earth elements, represent a focal point of research, primarily concentrated at the experimental stage with no successful clinical applications yet. A significant challenge is the differing metabolic processes and *in vivo* half-lives of the imaging groups within these probes.[102] Particularly, there is a notable mismatch in pharmacokinetics between short-lived radioactive isotopes, such as ^{68}Ga, and MRI imaging agents, which typically involve rare earth elements like gadolinium. Precisely controlling their metabolic processes to achieve synergistic imaging effects remains a formidable challenge.

These probes aim to leverage the complementary strengths of MRI's superior spatial resolution and soft tissue contrast with PET's acute sensitivity to metabolic activities.[103] However, synchronizing these modalities, which involves aligning the biological behaviours and decay rates of diverse imaging components, including rare earth elements, demands innovative solutions. Research is directed not only towards enhancing diagnostic accuracy but also towards optimizing the functional delivery and imaging capabilities of the probes within the human body's dynamic environment.

Advancements may rely on the development of new chelating agents that effectively bind and stabilize both MRI and PET components, harmonizing their interactions and extending the effective imaging window.[104] Additionally, the integration of advanced computational models to predict and manage the probes' behaviour *in vivo* could facilitate breakthroughs that transition experimental successes to clinical viability.[105] The ultimate goal is to develop dual-modality probes that effectively diagnose and guide therapeutic interventions, thus revolutionizing the field of medical imaging and treatment with the strategic use of REE.

4.3. Application of rare earth complexes as dual-modality molecular probes in MRI/CT

Computed tomography (CT), widely used in diagnostic imaging, capitalizes on the distinct X-ray absorption differences between healthy and pathological tissues to produce high-resolution 3D images.[106] The capability of CT to resolve soft tissues, however, is constrained due to their similar electron densities. Moreover, traditional CT imaging agents, predominantly iodine-based, exhibit limited sensitivity towards soft tissues and operate within brief imaging windows, which restricts their utility in detailed tumour diagnostics.[107,108] On the other hand, MRI, frequently utilizing REE such as gadolinium, excels in deep penetration and detailed soft tissue imaging, establishing it as the preferred technique for cancer and cardiovascular imaging.[109] By integrating MRI with CT, the combined strengths of both modalities can be leveraged, thus providing more precise and comprehensive diagnostic insights.

Gadolinium-based metal organic framework (MOF) nanoparticles are noted for their adjustable sizes and high loadings of gadolinium Gd(III), providing extended retention times and improved relaxivity, making them promising for overcoming the limitations faced by traditional Gd(III) complex molecular probes.[110] Tian[69] first reported on the synthesis of MRI/CT dual-modality molecular probes by combining GdMOF nanoparticles with gold nanoparticles (AuNPs). This process involved depositing polyacrylic acid (PAA) on the GdMOF nanoparticles' surface, followed by the coordination and reduction of Au ions, leading to the successful synthesis of the Gd-PAA-Au nanoprobe. PAA played a crucial role in facilitating the formation of highly dispersed AuNPs, averaging 4 nm in diameter on the GdMOF surfaces, which not only acted as bridges for the AuNPs but also enhanced water molecule access to interact with Gd^{3+} ions. The MRI results showed that this probe's longitudinal relaxivity (r_1) reached 4.9 mM^{-1} s^{-1}, closely matching that of unmodified GdMOF nanoparticles (r_1 = 4.5 mM^{-1} s^{-1}) and outperforming clinical nanoparticle probes, while also enhancing CT imaging contrast at a low Au concentration of 1.66 mg ml^{-1}. Furthermore, Lu[72] designed a dual-modality MRI/CT molecular probe, $NaGdF_4$:Dy@PDA-PEG-FA ($NaGdF_4$:Dy@PPF), which exhibits significant T_1 and T_2 relaxation properties. This probe was synthesized through a series of reactions including the thermal decomposition of gadolinium(III) hexahydrate and dysprosium(III) chloride, followed by the auto-polymerization of dopamine (DA) under alkaline conditions, Michael addition reaction, Schiff base reaction, and cyanodiimide conjugation. The inclusion of PDA, which has strong near-infrared absorption capabilities, and the doping of Gd^{3+} and Dy^{3+} ions, endow $NaGdF_4$: Dy@PPF with excellent photothermal conversion efficiency and enhanced T_1/T_2 weighted MRI and CT imaging capabilities. MTT assays, histological analyses, and mouse weight changes consistently indicate that the probe has relatively low cytotoxicity and negligible tissue damage. Moreover, under 808 nm irradiation, $NaGdF_4$: Dy@PPF exhibits pronounced photothermal cytotoxicity against 4T_1 cells and effectively inhibits tumour growth. All experimental results suggest that this multifunctional nanoprobe has the potential to serve as a novel dual-modality imaging probe, facilitating photothermal therapy (PTT) of tumours in mice under the guidance of multimodal imaging (Fig. 5).

Research into MRI/CT dual-modality molecular probes has increasingly focused on the development of nanoprobe

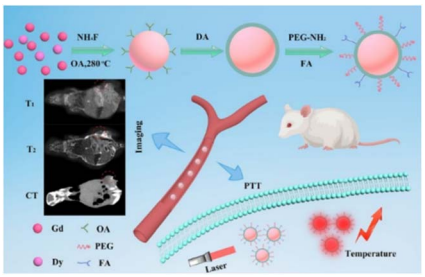

Fig. 5 Schematic illustration of the preparation of $NaGdF_4$: Dy@PPF as a therapeutic agent for multimodal imaging-guided PTT (adapted with permission ref. 72 with permission from the Royal Society of Chemistry, Copyright 2019).

technology, particularly those incorporating rare earth elements like gadolinium.[111] The biocompatibility of these nanomaterials is crucial for their clinical adoption, necessitating comprehensive investigations to assess their potential biotoxicity and ensure safety for human use.[112] Additionally, the complexity involved in fabricating these nanoparticle-based probes poses significant challenges, including the effective integration of both imaging modalities onto a single nanoparticle and the enhancement of the nanoprobe's size, water solubility, and biocompatibility.[113]

Advancements in nanoparticle probe design that seamlessly integrate the diagnostic capabilities of MRI and CT require innovative engineering approaches. These approaches should ensure the stabilization of nanoparticles in biological environments and optimize their interactions with body tissues to prevent adverse immune reactions. Moreover, improving the functional properties of these nanoparticles is essential for providing precise, reliable imaging crucial for accurate diagnostics and effective treatment planning.[114]

Future enhancements in MRI/CT dual-modality probes are likely to leverage the unique properties of lanthanide compounds, which enhance imaging quality due to their magnetic characteristics. Prioritizing the safety of these advanced materials is essential, necessitating extensive preclinical studies and clinical trials to fully verify their biocompatibility and effectiveness before they can be broadly implemented in clinical settings.

4.4. Application of rare earth complexes as dual-modality molecular probes in MRI/US

Ultrasound imaging operates based on the detection of reflected sound pulses, which are generated by a transducer and transmitted into tissues. These pulses are reflected based on the tissues' density and compressibility.[115] Ultrasound (US) is distinguished for its high spatiotemporal resolution, real-time imaging capabilities, absence of radiation, portability, and cost-effectiveness.[116] Ultrasound molecular probes typically consist of acoustically active microbubbles, ranging in size from several hundred nanometres to a few micrometers.[117] Despite its advantages, US is limited by its lower spatial resolution, which can restrict its utility. Combining MRI, which often incorporates rare earth elements like gadolinium to improve imaging contrast, with ultrasound can mitigate these limitations. This integration enables the rapid identification of tumours using ultrasound, followed using MRI to provide more detailed and accurate anatomical information.[118]

Conventional cancer treatments such as surgery, chemotherapy, and radiotherapy can cause significant damage to healthy tissues.[119,120] Photothermal therapy (PTT), which offers high specificity for targeting cancer cells, has emerged as a promising alternative. PTT employs photosensitizers to convert near-infrared (NIR) light into heat, selectively destroying cancerous tissues while sparing normal tissues due to rapid heat dissipation through blood circulation.[121,122] In a significant development, Li[81] created a novel multifunctional therapeutic agent by loading perfluorooctyl bromide (PFOB) into polylactic acid (PLA) nanocapsules (NCs), further enhanced with graphene oxide (GO) and gadolinium Gd(III) complex (GdDTPA). This integration of gadolinium enhances the NCs' capabilities as molecular probes, significantly improving both ultrasound (US) and Magnetic Resonance Imaging (MRI) performance. These gadolinium-doped NCs effectively destroy cancer cells under NIR laser exposure, combining real-time US imaging with high-resolution MRI to provide treatment without systemic damage. Additionally, cytotoxicity tests on HUVEC cells have confirmed the biocompatibility of these PFOB@PLA/GO/Gd-DTPANCs.

Building upon this, Shi[82] successfully synthesized a dual-modality molecular probe, PFP/GdDTPA/ICG@PLGA NPs (PGINPs), using a double emulsion method. This involved encapsulating GdDTPA, perfluoropentane (PFP), and indocyanine green (ICG) within a poly (lactic-*co*-glycolic acid) (PLGA) shell. Under near-infrared laser irradiation, the photosensitizer ICG effectively induces cancer cell death through photothermal therapy (PPT) and photodynamic therapy (PDT), without affecting normal tissues. The rapid temperature increase facilitates the conversion of PFP into bubbles, thereby enhancing ultrasound imaging capabilities. Concurrently, the released Gd-DTPA from PGINPs enhances penetration into cancerous tissues, leading to more uniform Magnetic Resonance Imaging outcomes. Structural characterization confirms that PGINPs possess a uniform particle size and high stability. Additionally, a 21 days *in vivo* toxicity study in healthy nude mice demonstrated that various dosages of PGINPs exhibit negligible toxicity. Thus, PGINPs hold significant clinical potential for ultrasound and MRI imaging and treatment of breast cancer.

The MRI/US dual-modality molecular probes discussed above highlight the extensive capabilities of rare earth elements to not only provide imaging of lesions or targeted areas but also to facilitate targeted therapeutic interventions. This integrated diagnostic and therapeutic approach, often referred to as "theranostics," holds substantial promise for enhancing patient care.[123] By incorporating rare earth elements, these probes can offer precise, real-time imaging while administering localized treatment, potentially revolutionizing the management of various diseases, particularly in oncology. It is anticipated that with ongoing advancements and rigorous clinical testing, this technology could soon be implemented in clinical practice, significantly improving patient survival and quality of life.[124]

The transition from experimental applications to routine clinical use is expected to provide a more targeted and efficient treatment regimen with fewer side effects compared to conventional methods.

5. Conclusion and future prospects

The integration of REE within various dual-modality molecular probes has significantly advanced diagnostic and therapeutic imaging capabilities. Systems such as MRI/US, MRI/CT, MRI/OI, and MRI/PET leverage the unique properties of elements like gadolinium to enhance image quality and therapeutic accuracy. Beyond these discussed modalities, rare earth elements are also being increasingly utilized in multimodal molecular probes, expanding their application scope and enhancing their utility in complex diagnostic and treatment scenarios.

Despite these advancements, the application of REE in dual-modality and multimodal molecular probes does not yet fully meet the ideal characteristics expected of molecular probes. Issues with biocompatibility, stability, and relaxivity of these probes are areas requiring further research and improvement. Additionally, the complex manufacturing processes, substantial costs, and stringent regulatory hurdles pose significant barriers to their broader clinical adoption.

Future research should focus on development of new compounds that can be used in more ideal dual-modality and multimodal molecular probes. While gadolinium has been predominantly employed in the development of dual-modality and multimodal molecular probes, the exploration and integration of other rare earth elements have been notably sparse. This underutilization represents a substantial area for academic and clinical research advancement. Future studies should prioritize the synthesis and characterization of novel compounds utilizing a broader spectrum of REE, which may exhibit unique physicochemical properties conducive to medical imaging and therapeutic applications. Investigating these elements could lead to significant enhancements in the functionality of molecular probes, potentially improving their biocompatibility, stability, and magnetic relaxivity. Such research efforts are crucial for expanding the repertoire of available molecular probes and may unveil innovative therapeutic modalities that could revolutionize precision medicine and diagnostic strategies.

Data availability

No primary research results, software or code have been included and no new data were generated or analysed as part of this review.

Author contributions

Jie-Fang He and Wen-Wen Yang: investigation and writing. Wen-Xuan Quan, Yue-Chun Yang and Zhengwei Zhang: discussion, editing of the manuscript. Qing-Ying Luo: writing reviewing and editing. All authors agree with the final form of a manuscript.

Conflicts of interest

The authors declare no conflict of interest.

Acknowledgements

This work was supported by the financial support of the Natural Science Foundation of China (21867005), Natural Science Foundation of Guizhou (QKH[2020]1Y430), Guizhou Scholarship for Overseas Students (GCCLXRC(2019)12), Research Project of Department of Education of Guangdong Province (2024KTSCX049), Science and Technology Project of Qiandongnan Prefecture (QDNKHZC[2021]06), Projects of Forestry Research in Guizhou Province (G[2022]TSLY07) and Guizhou Provincial Key Technology R&D Program (QKHZC[2022]131), GuangDong Basic and Applied Basic Research Foundation (2022A1515111228).

References

1 L. Omodara, S. Pitkäaho, E. M. Turpeinen, P. Saavalainen, K. Oravisjärvi and R. Keiski, *J. Cleaner Prod.*, 2019, **236**, 117573.
2 V. Balaram, *Geosci. Front.*, 2019, **10**, 1285–1303.
3 H. Peng, G. Ren, N. Hampp, A. Wu and F. Yang, *Nanoscale*, 2023, **15**, 10513–10528.
4 S. E. Crawford, P. R. Ohodnicki and J. P. Baltrus, *J. Mater. Chem. C*, 2020, **8**, 7975–8006.
5 H. Zhang and H. Zhang, *Light: Sci. Appl.*, 2022, **11**, 260.
6 F. Blancho, M. Davranche, R. Marsac, A. Léon, A. Dia, B. Grassl, S. Reynaud and J. Gigault, *Environ. Sci.: Nano*, 2022, **9**, 2094–2103.
7 U. Cho and J. K. Chen, *Cell Chem. Biol.*, 2020, **27**, 921–936.
8 G. S. Silva, J. D. L. Dutra, N. B. da Costa Jr, S. Alves Jr and R. O. Freire, *J. Phys. Chem. A*, 2020, **124**, 7678–7684.
9 Y. Ma, Y.-S. Yang, Y.-H. Jiang, Y.-X. Li, M. Liu, Z.-F. Li, H.-L. Han, Y.-P. Yang, X.-L. Xin and Q.-H. Jin, *RSC Adv.*, 2017, **7**, 41651–41666.
10 M. O. Barsukova, S. V. Cherezova, A. A. Sapianik, O. V. Lundovskaya, D. G. Samsonenko and V. P. Fedin, *RSC Adv.*, 2020, **10**, 38252–38259.
11 J. H. S. K. Monteiro, *Molecules*, 2020, **25**, 1–34.
12 W.-L. Zhou, Y. Chen, W. Lin and Y. Liu, *Chem. Commun.*, 2021, **57**, 11443–11456.
13 L. Labrador-Páez, E. C. Ximendes, P. Rodríguez-Sevilla, D. H. Ortgies, U. Rocha, C. Jacinto, E. Martín Rodríguez, P. Haro-González and D. Jaque, *Nanoscale*, 2018, **10**, 12935–12956.
14 J.-C. G. Bünzli, *Chem. Rev.*, 2010, **110**, 2729–2755.
15 X. Xu, H. Min and Y. Li, *Anal. Methods*, 2023, **15**, 5731–5753.
16 J.-C. G. Bünzli, *Coord. Chem. Rev.*, 2015, **293–294**, 19–47.
17 S. He, J. Song, J. Qu and Z. Cheng, *Chem. Soc. Rev.*, 2018, **47**, 4258–4278.

18 J. Meng, Y. Cui and Y. Wang, *J. Mater. Chem. B*, 2022, **10**, 8596–8615.
19 E. G. Moore, A. P. S. Samuel and K. N. Raymond, *Acc. Chem. Res.*, 2009, **42**, 542–552.
20 Y. Hasegawa, Y. Kitagawa and T. Nakanishi, *NPG Asia Mater.*, 2018, **10**, 52–70.
21 S. I. Weissman, *J. Chem. Phys.*, 1942, **10**, 214–217.
22 G. A. Crosby, R. E. Whan and R. M. Alire, *J. Chem. Phys.*, 1961, **34**, 743–748.
23 G. A. Crosby, R. E. Whan and J. J. Freeman, *J. Phys. Chem.*, 1962, **66**, 2493–2499.
24 R. E. Whan and G. A. Crosby, *J. Mol. Spectrosc.*, 1962, **8**, 315–327.
25 Y. Cui, Y. Yue, G. Qian and B. Chen, *Chem. Rev.*, 2012, **112**, 1126–1162.
26 S. I. Klink, L. Grave, D. N. Reinhoudt, F. C. J. M. van Veggel, M. H. V. Werts, F. A. J. Geurts and J. W. Hofstraat, *J. Phys. Chem. A*, 2000, **104**, 5457–5468.
27 E. B. Ehlerding, L. Sun, X. Lan, D. Zeng and W. Cai, *J. Nucl. Med.*, 2018, **59**, 390–395.
28 M. Rudin and R. Weissleder, *Nat. Rev. Drug Discovery*, 2003, **2**, 123–131.
29 C.-T. Yang, K. K. Ghosh, P. Padmanabhan, O. Langer, J. Liu, D. N. C. Eng, C. Halldin and B. Gulyás, *Theranostics*, 2018, **8**, 6210–6232.
30 W.-F. Lai, A. L. Rogach and W.-T. Wong, *Chem. Soc. Rev.*, 2017, **46**, 6379–6419.
31 B. Lin, F. Xiao, J. Jiang, Z. Zhao and X. Zhou, *Chem. Sci.*, 2023, **14**, 14039–14061.
32 D. Zhao, J. Cao, L. Zhang, S. Zhang and S. Wu, *Biosensors*, 2022, **12**, 1–33.
33 M. Li, Y. Wang, M. Liu and X. Lan, *Theranostics*, 2018, **8**, 2954–2973.
34 S. Yoon and J. J. Rossi, *Pharmaceuticals*, 2018, **11**, 1–16.
35 R. Weissleder and M. J. Pittet, *Nature*, 2008, **452**, 580–589.
36 S. Pan, A. Ding, Y. Li, Y. Sun, Y. Zhan, Z. Ye, N. Song, B. Peng, L. Li, W. Huang and H. Shao, *Chem. Soc. Rev.*, 2023, **52**, 5706–5743.
37 B. Brito, T. W. Price, J. Gallo, M. Bañobre-López and G. J. Stasiuk, *Theranostics*, 2021, **11**, 8706–8737.
38 J. Zhao, J. Chen, S. Ma, Q. Liu, L. Huang, X. Chen, K. Lou and W. Wang, *Acta Pharm. Sin. B*, 2018, **8**, 320–338.
39 E. Peng, F. Wang and J. M. Xue, *J. Mater. Chem. B*, 2015, **3**, 2241–2276.
40 T. Yousaf, G. Dervenoulas and M. Politis, *Int. Rev. Neurobiol.*, 2018, **141**, 31–76.
41 Z. Deng, D. Lu, S. Liu, X. Tan and G. Song, *Mater. Chem. Front.*, 2024, **8**, 248–264.
42 H.-K. Kim, G. Lee and Y. Chang, *Future Med. Chem.*, 2018, **10**, 639–661.
43 M. Wu and J. Shu, *Contrast Media Mol. Imaging*, 2018, **2018**, 1–12.
44 H. Du, Q. Wang, Z. Liang, Q. Li, F. Li and D. Ling, *Nanoscale*, 2022, **14**, 17483–17499.
45 A. Paterson and D. P. Frush, *Clin. Radiol.*, 2007, **62**, 507–517.
46 S. Shuvaev, E. Akam and P. Caravan, *Invest. Radiol.*, 2021, **56**, 20–34.
47 Q. Chen, H. Song, J. Yu and K. Kim, *Sensors*, 2021, **21**, 1–19.
48 L. J. Brattain, B. A. Telfer, M. Dhyani, J. R. Grajo and A. E. Samir, *Abdom. Radiol.*, 2018, **43**, 786–799.
49 H. Yao, J. Li, Y. Song, H. Zhao, Z. Wei, X. Li, Y. Jin, B. Yang and J. Jiang, *Int. J. Nanomed.*, 2018, **13**, 6249–6264.
50 Y.-H. Jin, Q.-F. Hua, J.-J. Zheng, X.-H. Ma, T.-X. Chen, S. Zhang, B. Chen, Q. Dai and X.-H. Zhang, *Cell. Physiol. Biochem.*, 2018, **49**, 271–281.
51 L. Zhong, H. Zou, Y. Huang, W. Gong, J. He, J. Tan, Z. Lai, Y. Li, C. Zhou, G. Zhang, G. Li, N. Yang and Y. Zhao, *J. Biomed. Nanotechnol.*, 2019, **15**, 352–362.
52 B.-B. Shang, X. Li, X.-R. Zhang, W.-S. Huang, B.-P. Qi and C.-H. Zhou, *Bioelectrochemistry*, 2019, **129**, 278–285.
53 Y. Wang, X. Wang, Q. Meng, H. Jia, R. Zhang, P. Zhu, R. Song, H. Feng and Z. Zhang, *Tetrahedron*, 2017, **73**, 5700–5705.
54 M. I. A. Pereira, G. Pereira, C. A. P. Monteiro, C. F. G. C. Geraldes, P. E. Cabral Filho, C. L. Cesar, A. A. de Thomaz, B. S. Santos, G. A. L. Pereira and A. Fontes, *Sci. Rep.*, 2019, **9**, 1–11.
55 R. Jouclas, S. Laine, S. V. Eliseeva, J. Mandel, F. Szeremeta, P. Retailleau, J. He, J. F. Gallard, A. Pallier, C. S. Bonnet, S. Petoud, P. Durand and É. Tóth, *Angew. Chem., Int. Ed.*, 2024, **63**, e202317728.
56 X. Yu, X. Yuan, Z. Huang, W. Zhang, F. Huang and L. Ren, *ACS Biomater. Sci. Eng.*, 2020, **6**, 6405–6414.
57 Y. Huang, L. Li, D. Zhang, L. Gan, P. Zhao, Y. Zhang, Q. Zhang, M. Hua and C. Jia, *Magn. Reson. Imaging*, 2020, **68**, 113–120.
58 J. Yin, Y. Zhang, D. Ma, R. Yang, F. Xu, H. Wu, C. He, L. Liu, J. Dong and Y. Shao, *ACS Appl. Mater. Interfaces*, 2019, **11**, 41069–41081.
59 Y. Pan, W. Chen, J. Yang, J. Zheng, M. Yang and C. Yi, *Anal. Chem.*, 2018, **90**, 1992–2000.
60 F. Oukhatar, S. V. Eliseeva, C. S. Bonnet, M. Placidi, N. K. Logothetis, S. Petoud, G. Angelovski and É. Tóth, *Inorg. Chem.*, 2019, **58**, 13619–13630.
61 S. Huang, P. Chen and C. Xu, *Talanta*, 2017, **165**, 161–166.
62 M. Harris, C. Henoumont, W. Peeters, S. Toyouchi, L. Vander Elst and T. N. Parac-Vogt, *Dalton Trans.*, 2018, **47**, 10646–10653.
63 A. Kumar, S. Zhang, G. Hao, G. Hassan, S. Ramezani, K. Sagiyama, S.-T. Lo, M. Takahashi, A. D. Sherry, O. K. Öz, Z. Kovacs and X. Sun, *Bioconjugate Chem.*, 2015, **26**, 549–558.
64 D. Chen, Y. Zhou, D. Yang, M. Guan, M. Zhen, W. Lu, M. E. Van Dort, B. D. Ross, C. Wang, C. Shu and H. Hong, *ACS Appl. Mater. Interfaces*, 2019, **11**, 21343–21352.
65 D. Vecchione, M. Aiello, C. Cavaliere, E. Nicolai, P. Netti and E. Torino, *Nanomedicine*, 2017, **12**, 2223–2231.
66 H. F. Schmitthenner, T. M. Barrett, S. A. Beach, L. E. Heese, C. Weidman, D. E. Dobson, E. R. Mahoney, N. C. Schug, K. G. Jones, C. Durmaz, O. Otasowie, S. Aronow, Y. P. Lee, H. D. Ophardt, A. E. Becker, J. P. Hornak, I. M. Evans and M. C. Ferran, *ACS Appl. Bio Mater.*, 2021, **4**, 5435–5448.
67 N. Vologdin, G. A. Rolla, M. Botta and L. Tei, *Org. Biomol. Chem.*, 2013, **11**, 1683–1690.

68 C. Truillet, P. Bouziotis, C. Tsoukalas, J. Brugiere, M. Martini, L. Sancey, T. Brichart, F. Denat, F. Boschetti, U. Darbost, I. Bonnamour, D. Stellas, C. D. Anagnostopoulos, V. Koutoulidis, L. A. Moulopoulos, P. Perriat, F. Lux and O. Tillement, *Contrast Media Mol. Imaging*, 2015, **10**, 309–319.
69 C. Tian, L. Zhu, F. Lin and S. G. Boyes, *ACS Appl. Mater. Interfaces*, 2015, **7**, 17765–17775.
70 S. Mastrogiacomo, A. E. Kownacka, W. Dou, B. P. Burke, R. T. M. de Rosales, A. Heerschap, J. A. Jansen, S. J. Archibald and X. F. Walboomers, *Adv. Healthcare Mater.*, 2018, **7**, 1800202.
71 M. Yang, X. Wang, F. Pu, Y. Liu, J. Guo, S. Chang, G. Sun and Y. Peng, *Pharmaceutics*, 2021, **13**, 1593.
72 W. Lu, Y. Liao, C. Jiang, R. Wang, X. Shan, Q. Chen, G. Sun and J. Liu, *New J. Chem.*, 2019, **43**, 7371–7378.
73 Q. Yin, X. Jin, G. Yang, C. Jiang, Z. Song and G. Sun, *RSC Adv.*, 2014, **4**, 53561–53569.
74 X. Jin, F. Fang, J. Liu, C. Jiang, X. Han, Z. Song, J. Chen, G. Sun, H. Lei and L. Lu, *Nanoscale*, 2015, **7**, 15680–15688.
75 C. Yang, T. Mei, Q. Fu, Y. Zhang, Y. Liu, R. Cui, G. Li, Y. Wang, J. Huang, J. Jia, B. Chen and Y. Hu, *J. Funct. Biomater.*, 2022, **13**, 87.
76 B. Zhou, Z. Xiong, P. Wang, C. Peng, M. Shen, S. Mignani, J. P. Majoral and X. Shi, *Drug Delivery*, 2018, **25**, 178–186.
77 J. Liu, Z. Xiong, J. Zhang, C. Peng, B. Klajnert-Maculewicz, M. Shen and X. Shi, *ACS Appl. Mater. Interfaces*, 2019, **11**, 15212–15221.
78 Y. Feng, H. Chen, B. Shao, S. Zhao, Z. Wang and H. You, *ACS Appl. Mater. Interfaces*, 2018, **10**, 25511–25518.
79 Z. Wei, M. Wu, Z. Li, Z. Lin, J. Zeng, H. Sun, X. Liu, J. Liu, B. Li and Y. Zeng, *Drug Delivery*, 2018, **25**, 353–363.
80 M. W. Ahmad, W. Xu, S. J. Kim, J. S. Baeck, Y. Chang, J. E. Bae, K. S. Chae, J. A. Park, T. J. Kim and G. H. Lee, *Sci. Rep.*, 2015, **5**, 8549.
81 Z. Li, H. Ke, J. Wang, Z. Miao and X. Yue, *J. Nanosci. Nanotechnol.*, 2016, **16**, 2201–2209.
82 M. Shi, F. Zuo, Y. Tao, Y. Liu, J. Lu, S. Zheng, J. Lu, P. Hou, J. Li and K. Xu, *Colloids Surf., B*, 2020, **196**, 111278.
83 F. Maghsoudinia, M. B. Tavakoli, R. K. Samani, S. H. Hejazi, T. Sobhani, F. Mehradnia and M. A. Mehrgardi, *Talanta*, 2021, **228**, 122245.
84 F. Maghsoudinia, H. Akbari-Zadeh, M. Aminolroayaei, F. F. Birgani,, A. Shanei and R. K. Samani, *Eur. J. Pharm. Sci.*, 2022, **174**, 106207.
85 S. P. Rowe and M. G. Pomper, *Ca-Cancer J. Clin.*, 2021, **72**, 333–352.
86 L. Omodara, S. Pitkäaho, E.-M. Turpeinen, P. Saavalainen, K. Oravisjärvi and R. Keiski, *J. Cleaner Prod.*, 2019, **236**, 117573.
87 W. Mnasri, M. Parvizian and S. Ammar-Merah, *Nanomaterials*, 2021, **11**, 354.
88 G. M. Albuquerque, I. Souza-Sobrinha, S. D. Coiado, B. S. Santos, A. Fontes, G. A. L. Pereira and G. Pereira, *Top. Curr. Chem.*, 2021, **379**, 12.
89 T. Terai and T. Nagano, *Pfluegers Arch.*, 2013, **465**, 347–359.
90 E. A.-O. Gómez-González, C. A.-O. Caro, M. A.-O. García-Martín, A. A.-O. Becerro and M. A.-O. X. Ocaña, *Nanoscale*, 2022, **14**, 11461–11470.
91 C. Y. Liu, Z. Y. Gao, J. F. Zeng, Y. Hou, F. Fang, Y. L. Li, R. R. Qiao, L. Shen, H. Lei, W. S. Yang and M. Y. Gao, *ACS Nano*, 2013, **7**, 7227–7240.
92 Q. Ma, J. Wang, Z. Li, X. Lv, L. Liang and Q. A.-O. X. Yuan, *Small*, 2019, **15**, 1804969.
93 C. Do, J. DeAguero, A. Brearley, X. Trejo, T. Howard, G. P. Escobar and B. Wagner, *Kidney360*, 2020, **1**, 561–568.
94 R. C. Somers, M. G. Bawendi and D. G. Nocera, *Chem. Soc. Rev.*, 2007, **36**, 579–591.
95 M. J. Ruedas-Rama, J. D. Walters, A. Orte and E. A. H. Hall, *Anal. Chim. Acta*, 2012, **751**, 1–23.
96 O. Gordon, C. A. Ruiz-Bedoya, A. A. Ordonez, E. W. Tucker and S. K. Jain, *mBio*, 2019, **10**, e00317.
97 A. W. Sauter, H. F. Wehrl, A. Kolb, M. S. Judenhofer and B. J. Pichler, *Trends Mol. Med.*, 2010, **16**, 508–515.
98 T. R. Goodman, A. Mustafa and E. Rowe, *Pediatr. Radiol.*, 2019, **49**, 469–478.
99 S. C. Chawla, N. C. Federman, D. Zhang, K. Nagata, S. Nuthakki, M. F. McNitt-Gray and M. I. J. P. R. Boechat, *Pediatr. Radiol.*, 2009, **40**, 681–686.
100 T. E. Yankeelov, T. E. Peterson, R. G. Abramson, D. Izquierdo-Garcia, L. R. Arlinghaus, X. Li, N. C. Atuegwu, C. Catana, H. C. Manning, Z. A. Fayad and J. C. Gore, *Magn. Reson. Imaging*, 2012, **30**, 1342–1356.
101 E. Lennie, C. Tsoumpas and S. Sourbron, *EJNMMI Phys.*, 2021, **8**, 62.
102 P. Kush, P. Kumar, R. Singh and A. Kaushik, *Asian J. Pharm. Sci.*, 2021, **16**, 704–737.
103 A. Kastelik-Hryniewiecka, P. Jewula, K. Bakalorz, G. Kramer-Marek and N. Kuźnik, *Int. J. Nanomed.*, 2022, **16**, 8465–8483.
104 H. Liu, R. Wang, H. Gao, L. Chen, X. Li, X. Yu, Y. Wu, Y. Bai, W. Wei and M. Wang, *Adv. Ther.*, 2023, **7**, 2300232.
105 M. Aiello, C. Cavaliere, R. Marchitelli, A. d'Albore, E. De Vita and M. Salvatore, *Int. Rev. Neurobiol.*, 2018, **141**, 97–128.
106 M. M. Lell and M. Kachelrieß, *Invest. Radiol.*, 2020, **55**, 8–19.
107 H. Alkadhi and A. Euler, *Invest. Radiol.*, 2020, **55**, 545–555.
108 Y. Liu, K. Ai and L. Lu, *Acc. Chem. Res.*, 2012, **45**, 1817–1827.
109 J. Pellico, C. M. Ellis and J. J. Davis, *Contrast Media Mol. Imaging*, 2019, **2019**, 1845637.
110 D. Giliopoulos, A. Zamboulis, D. Giannakoudakis, D. Bikiaris and K. Triantafyllidis, *Molecules*, 2020, **25**, 1–38.
111 N. Liu, C. Homann, S. Morfin, M. S. Kesanakurti, N. D. Calvert, A. J. Shuhendler, T. Al and E. Hemmer, *Nanoscale*, 2023, **15**, 19546–19556.
112 V. J. X. Phua, C.-T. Yang, B. Xia, S. X. Yan, J. Liu, S. E. Aw, T. He and D. C. E. Ng, *Nanomaterials*, 2022, **12**, 582.
113 Z. Gao, T. Ma, E. Zhao, D. Docter, W. Yang, R. H. Stauber and M. Gao, *Small*, 2015, **12**, 556–576.
114 J. Wan, X. Zhang, K. Zhang and Z. Su, *Rev. Anal. Chem.*, 2020, **39**, 209–221.
115 R. Gessner and P. A. Dayton, *Mol. Imaging*, 2010, **9**, 117–127.
116 A. Zlitni and S. S. Gambhir, *Curr. Opin. Chem. Biol.*, 2018, **45**, 113–120.

117 G. Zhang, H.-R. Ye, Y. Sun and Z.-Z. Guo, *ACS Sens.*, 2022, **7**, 2857–2864.
118 D. A. Feinberg, D. Giese, D. A. Bongers, S. Ramanna, M. Zaitsev, M. Markl and M. Günther, *Magn. Reson. Med.*, 2009, **63**, 290–296.
119 L. P. Wallner, Y. Li, M. C. McLeod, J. Gargaro, A. W. Kurian, R. Jagsi, A. Radhakrishnan, A. S. Hamilton, K. C. Ward, S. T. Hawley and S. J. Katz, *Cancer*, 2019, **125**, 1815–1822.
120 C. Fletcher, C. Wilson, A. D. Hutchinson and E. A. Grunfeld, *Cancer Treat. Rev.*, 2018, **68**, 86–93.
121 C. Huang, J. Feng, J. Zhou, H. Xiang, K. Deng and E. Kan, *J. Am. Chem. Soc.*, 2019, **141**, 12413–12418.
122 Y. Cao, X. Meng, D. Wang, K. Zhang, W. Dai, H. Dong and X. Zhang, *ACS Appl. Mater. Interfaces*, 2018, **10**, 17732–17741.
123 A. Józefczak, K. Kaczmarek and R. Bielas, *Theranostics*, 2021, **11**, 10091–10113.
124 M. Gu, W. Li, L. Jiang and X. Li, *Acta Biomater.*, 2022, **148**, 22–43.